CrossMark

Optimal Energy Growth in Current Sheets

David MacTaggart[1] (iD) · Peter Stewart[1] (iD)

Abstract In this article, we investigate the possibility of transient growth in the linear perturbation of current sheets. The resistive magnetohydrodynamics operator for a background field consisting of a current sheet is non-normal, meaning that associated eigenvalues and eigenmodes can be very sensitive to perturbation. In a linear stability analysis of a tearing current sheet, we show that modes that are damped as $t \rightarrow \infty$ can produce transient energy growth, contributing faster growth rates and higher energy attainment (within a fixed finite time) than the unstable tearing mode found from normal-mode analysis. We determine the transient growth for tearing-stable and tearing-unstable regimes and discuss the consequences of our results for processes in the solar atmosphere, such as flares and coronal heating. Our results have significant potential impact on how fast current sheets can be disrupted. In particular, transient energy growth due to (asymptotically) damped modes may lead to accelerated current sheet thinning and, hence, a faster onset of the plasmoid instability, compared to the rate determined by the tearing mode alone.

Keywords Magnetohydrodynamics · Instabilities · Magnetic reconnection, theory

1. Introduction

The prototypical instability in resistive magnetohydrodynamics (MHD) is the tearing instability. As the name suggests, this instability describes the growth of the "tearing" of a magnetic field or, to be more precise, the change in the field's magnetic topology. In two dimensions, the tearing instability creates a series of magnetic islands, similar to Kelvin's cat's eyes (*e.g.* Schindler, 2006). In three dimensions, the change in magnetic topology can be more complicated (*e.g.* Priest, 2014).

The standard magnetic field configuration for the tearing instability is the current sheet. The name derives from a thin layer of intense (compared to the surrounding environment) current density located in a highly sheared magnetic field. Normally, the magnetic field

---

✉ D. MacTaggart
   david.mactaggart@glasgow.ac.uk

[1] School of Mathematics & Statistics, University of Glasgow, Glasgow G12 8SQ, UK

points in opposite directions on either side of the current sheet, with the width of the current sheet (where the change takes place) being much smaller than the typical length scale of the large-scale system.

Since the seminal work of Furth, Kileen, and Rosenbluth (1963), there have been many studies of the tearing instability that consider effects such as different geometries or the inclusion of extra physics (*e.g.* Pritchett, Lee, and Drake, 1980; Terasawa, 1983; Tassi, Hastie, and Porcelli, 2007; Tenerani *et al.*, 2015). In the context of solar physics, magnetic reconnection (the change of magnetic topology) is a fundamental physical process, so the tearing instability is of great interest in this field. Solar eruptions, ranging from flares to jets to coronal mass ejections (CMEs), are often believed to be triggered by magnetic reconnection (*e.g.* MacNeice *et al.*, 2004; MacTaggart and Haynes, 2014; MacTaggart *et al.*, 2015). MHD simulations have demonstrated that fast eruptive behavior is strongly linked to the tearing of current sheets.

Although large-scale MHD simulations, such as those cited above, can describe the nonlinear evolution of the tearing instability, they are not so effective when it comes to analyzing the onset of instability. The complex geometries, sensitivity to boundary conditions, and low (compared to the corona) Lundquist numbers make a detailed analysis of the onset of instability very challenging. Therefore, studies that focus only on the (linear) onset of the instability are still very important.

When studying the onset of the tearing instability, the vast majority of studies have focused on normal-mode analysis (*e.g.* Chandrasekhar, 1961). That is, solutions are sought with a time dependence of the form

$$\phi \sim \exp(-i\omega t), \tag{1}$$

where ϕ represents a variable of the system, ω is the frequency, and t is time. If $\Im(\omega) > 0$, then ϕ grows exponentially as $t \to \infty$. Otherwise, if $\Im(\omega) < 0$, then ϕ decays exponentially as $t \to \infty$. The objective of normal-mode analysis is to find the highest value of $\Im(\omega)$ that corresponds to the fastest growing mode. The onset of the instability can, therefore, be recast as an eigenvalue problem for eigenvalues ω. For the tearing instability, there is one eigenvalue such that $\Im(\omega) > 0$. Hence, there is only one mode that causes exponential growth in the linearized system, and it is referred to as the tearing mode. It can be shown analytically (Furth, Kileen, and Rosenbluth, 1963; Schindler, 2006) that the growth rate of the tearing mode depends on the magnetic Lundquist number S (which we define later) in the form $S^{-\alpha}$, where $0 < \alpha < 1$. For environments such as the solar corona, where the magnetic Lundquist number is $O(10^8)$ and above (*e.g.* Hood and Hughes, 2011), the tearing mode growth rate is very slow compared to rapidly occurring phenomena like flares. This has led researchers to study the nonlinear tearing instability in order to find faster dynamics. However, it may be the case that a faster onset of the instability can be found in the analysis of the linearized system by including the energy growth that is ignored by normal-mode analysis.

As mentioned above, eigenvalues describe the behavior of growth or decay as $t \to \infty$. In normal-mode analysis, all eigenvalues satisfying $\Im(\omega) < 0$ (exponential decay) are ignored. However, modes associated with these rejected eigenvalues can produce transient growth, which, although it decays exponentially as $t \to \infty$, can produce significant energy growth within a finite time. If this transient growth is large enough, the growth of the linear system could enter the nonlinear regime much faster than by the growth rate of the tearing mode alone. Therefore, the transient growth due to the damped modes of the system could lead to current sheet disruption much faster than by the growth rate of the (unstable) tearing mode.

There has been much interest in the study of transient growth of the linearized Navier–Stokes equations for shear flows (*e.g.* Reddy and Henningson, 1993; Reddy, Schmid, and Henningson, 1993; Schmid and Henningson, 1994; Hanifi, Schmid, and Henningson, 1996). Mathematically, transient growth corresponds to the non-normality of the system. A non-normal system is characterized by the non-orthogonality of eigenmodes. To analyze the non-normal behavior of such systems, a generalization of the eigenvalue spectrum, known as the pseudospectrum, can be used (Trefethen and Embree, 2005). Bobra *et al.* (1994) used pseudospectra to relate ideal and resistive MHD spectra. They showed that the resistive MHD eigenmodes, for sheared background fields, are strongly non-orthogonal and, hence, can exhibit transient growth. The effects of non-normal behavior in MHD have also been studied in the context of magnetic field generation (*e.g.* Farrell and Ioannou, 1999a,b; Livermore and Jackson, 2006). In solar physics, transient energy growth has attracted attention in solar wind applications (*e.g.* Camporeale, Burgess, and Passot, 2009; Camporeale, 2010).

The effects of non-normal behavior have not, to our knowledge, been applied to eruptive behavior in the corona, which is the focus of this article. By considering a sheared background magnetic field (a current sheet), we study the effects of transient behavior in the cases when the system is (spectrally) stable and unstable to the tearing instability. We illustrate the non-normality of the associated operator using a particular form of the pseudospectrum that is simple to calculate once the eigenvalue spectrum has been obtained. The article is outlined as follows: the initial model equations and boundary conditions are introduced, the background theory for calculating the optimal energy growth is discussed, the spectra and energy growth envelopes are displayed for several cases, and the article concludes with a discussion of potential applications and further work.

2. Model Description

To study the tearing instability, we consider the 2D incompressible MHD equations

$$\rho \left(\frac{\partial \boldsymbol{u}}{\partial t} + (\boldsymbol{u} \cdot \nabla)\boldsymbol{u} \right) = -\nabla p + \mu^{-1}(\nabla \times \boldsymbol{B}) \times \boldsymbol{B}, \tag{2}$$

$$\frac{\partial \boldsymbol{B}}{\partial t} = \nabla \times (\boldsymbol{u} \times \boldsymbol{B}) + \eta \nabla^2 \boldsymbol{B}, \tag{3}$$

$$\nabla \cdot \boldsymbol{B} = \nabla \cdot \boldsymbol{u} = 0, \tag{4}$$

where $\boldsymbol{B}$ is the magnetic field, $\boldsymbol{u}$ is the velocity, ρ is the (constant) density, p is the plasma pressure, η is the constant magnetic diffusivity, and μ is the magnetic permeability. Although compressible MHD would be a more suitable model for the solar atmosphere, we chose to use incompressible MHD for two reasons. The first reason is simplicity – to illustrate our procedure, incompressible MHD allows for an obvious measure of the disturbance energy. The theory that we develop, however, could be extended to compressible MHD and more complicated models. The second reason is that most of the literature on the tearing instability uses incompressible MHD. Therefore, comparison with previous work can be made more directly.

Our background (static) equilibrium is

$$p_0 = p_0(x), \qquad \boldsymbol{B}_0 = B_{0z}(x)\boldsymbol{e}_z, \qquad \boldsymbol{u}_0 = \boldsymbol{0}, \tag{5}$$

where the zero subscript corresponds to the equilibrium and

$$p_0(x) + \frac{1}{2\mu}B_{0z}^2(x) = \text{const.} \tag{6}$$

Before choosing a particular form for $B_{0z}(x)$, let us linearize the MHD equations. Setting $(\boldsymbol{u}, \boldsymbol{B}, p) = (\boldsymbol{u}_0, \boldsymbol{B}_0, p_0) + (\boldsymbol{u}_1, \boldsymbol{B}_1, p_1)$ results in the linearization

$$\rho\frac{\partial \boldsymbol{u}_1}{\partial t} = -\nabla p_1 + \mu^{-1}(\nabla \times \boldsymbol{B}_1) \times \boldsymbol{B}_0 + \mu^{-1}(\nabla \times \boldsymbol{B}_0) \times \boldsymbol{B}_1, \tag{7}$$

$$\frac{\partial \boldsymbol{B}_1}{\partial t} = \nabla \times (\boldsymbol{u}_1 \times \boldsymbol{B}_0) + \eta\nabla^2 \boldsymbol{B}_1, \tag{8}$$

$$\nabla \cdot \boldsymbol{B}_1 = \nabla \cdot \boldsymbol{u}_1 = 0. \tag{9}$$

Note that we are assuming $\eta \ll 1$, which is typical in many solar and astrophysical applications. We therefore ignore the contribution of diffusion on the background equilibrium in Equation 8, expecting the dynamics of the instability to occur on a much shorter timescale than the diffusion time.

We now look for solutions of the form

$$\boldsymbol{u}_1 = \left[u(x, t), 0, u_z(x, t)\right]^{\text{T}} e^{ikz}, \qquad \boldsymbol{B}_1 = \left[b(x, t), 0, b_z(x, t)\right]^{\text{T}} e^{ikz}, \tag{10}$$

where k is the wavenumber of disturbances in the z-direction. Taking the curl of Equation 7, we eliminate p_1. Using the solenoidal constraints in Equation 9, we can eliminate u_z and b_z. This leaves

$$\frac{\partial}{\partial t}\left(\frac{\partial^2 u}{\partial x^2} - k^2 u\right) = \frac{ikB_{0z}}{\mu\rho}\left(\frac{\partial^2 b}{\partial x^2} - k^2 b\right) - \frac{ikB_{0z}''}{\mu\rho}b, \tag{11}$$

$$\frac{\partial b}{\partial t} = ikB_{0z}u + \eta\left(\frac{\partial^2 b}{\partial x^2} - k^2 b\right), \tag{12}$$

where a prime denotes differentiation with respect to x.

2.1. Equilibrium

We chose a classic form for the background magnetic field known as the Harris sheet. The magnetic field of the Harris sheet is given by

$$B_{0z}(x) = B_0 \tanh\left(\frac{x}{x_0}\right), \qquad B_{0z}''(x) = -\frac{B_0}{x_0^2}\frac{2}{\cosh^2(x/x_0)}\tanh\left(\frac{x}{x_0}\right), \tag{13}$$

where B_0 is the maximum field strength and x_0 measures the thickness of the current sheet. The equilibrium pressure then comes from Equation 6, but is not important for our calculations.

2.2. Non-dimensionalization

To non-dimensionalize the equations, consider

$$u = u_0 u^*, \qquad b = B_0 b^*, \qquad t = t_0 t^*, \qquad x = x_0 x^*, \tag{14}$$

with

$$t_0 = \frac{x_0}{u_0}, \quad u_0 = \frac{B_0}{\sqrt{\mu \rho}}, \tag{15}$$

where u_0 is the Alfvén speed. The linearized MHD equations become (after dropping the asterisks)

$$\frac{\partial}{\partial t} \left(\frac{\partial^2 u}{\partial x^2} - k^2 u \right) = ik B_{0z} \left(\frac{\partial^2 b}{\partial x^2} - k^2 b \right) - ik B_{0z}'' b, \tag{16}$$

$$\frac{\partial b}{\partial t} = ik B_{0z} u + S^{-1} \left(\frac{\partial^2 b}{\partial x^2} - k^2 b \right), \tag{17}$$

where

$$S = \frac{x_0 u_0}{\eta} \tag{18}$$

is the (non-dimensional) Lundquist number.

2.3. Boundary Conditions

We require that $b \to 0$ and $u \to 0$ as $x \to \pm\infty$. However, since numerical simulations typically range between finite values, we approximate the boundary conditions as $b = u = 0$ at $x = \pm d$ for some $d > 0$. This approach makes comparisons to simulations of tearing instabilities more feasible. Moreover, since the tearing instability develops in a thin boundary layer near $x = 0$, a value of d much higher than the width of the boundary layer will result in a good approximation. In the Appendix, we perform one of our subsequent calculations in the half-plane $(x, z) \in [0, \infty) \times (-\infty, \infty)$. Comparing this to the corresponding result from the closed domain reveals that the exact form of the boundary conditions is not of vital importance for the results of this article.

3. Background Theory

In this section we discuss the background theory for determining the optimal energy growth and how non-normal contributions are included. Our aim is to solve the full initial value problem, rather than just the eigenvalue problem. However, in order to determine the effects of different modes on energy growth, we recast the initial value problem in terms of a selection of eigenvalues and (corresponding) eigenmodes. By considering the kinetic and magnetic energies, we define a (physically) suitable norm for the system and use this to determine the optimal energy growth.

3.1. Operator Equations

In anticipation of the numerical approach that we describe later, we write the linearized MHD equations as a matrix–vector system. Equations 16 and 17 can be written in the form

$$\frac{\partial}{\partial t} \mathcal{M} \boldsymbol{v} = \mathcal{L} \boldsymbol{v}, \tag{19}$$

with

$$\mathcal{M} = \begin{pmatrix} \mathcal{D}^2 - k^2 & 0 \\ 0 & \mathcal{I} \end{pmatrix}, \qquad \mathcal{L} = \begin{pmatrix} 0 & \mathcal{L}_I \\ ikB_z & \mathcal{L}_R \end{pmatrix}, \qquad \boldsymbol{v} = \begin{pmatrix} u \\ b \end{pmatrix}, \tag{20}$$

and

$$\mathcal{L}_I = ikB_z(\mathcal{D}^2 - k^2) - ikB_z'', \qquad \mathcal{L}_R = S^{-1}(\mathcal{D}^2 - k^2), \qquad \mathcal{D} = \frac{\partial}{\partial x}, \tag{21}$$

where $\mathcal{I}$ represents the identity operator. If we consider solutions of the form

$$\boldsymbol{v} = \widetilde{\boldsymbol{v}} \exp(-i\omega t), \quad \omega \in \mathbb{C}, \tag{22}$$

we can transform the initial value problem of Equation 19 into the generalized eigenvalue problem

$$-i\omega\mathcal{M}\widetilde{\boldsymbol{v}} = \mathcal{L}\widetilde{\boldsymbol{v}}. \tag{23}$$

Making the assumption of Equation 22 restricts us to examining growth or decay in the limit $t \to \infty$ only. In normal-mode analysis, we would solve Equation 23 for the eigenvalue with the highest value of $\Im(\omega) > 0$. This approach, however, misses the possibility of transient growth due to eigenmodes with corresponding eigenvalues satisfying $\Im(\omega) < 0$, *i.e.* damped modes.

In our calculations of transient growth, we made use of the eigenvalue spectrum calculated from Equation 23 and the corresponding eigenmodes. In practice, however, we only need to consider a finite number of eigenmodes since not all eigenfunctions will contribute non-normal behavior. Therefore, we restrict ourselves to the space $\mathbb{S}^N$ spanned by the first N least damped eigenmodes of $\mathcal{M}^{-1}\mathcal{L}$:

$$\mathbb{S}^N = \mathrm{span}\{\widetilde{\boldsymbol{v}}_1, \ldots, \widetilde{\boldsymbol{v}}_N\}. \tag{24}$$

We expand the vector functions $\boldsymbol{v} \in \mathbb{S}^N$ in terms of the basis $\{\widetilde{\boldsymbol{v}}_1, \ldots, \widetilde{\boldsymbol{v}}_N\}$:

$$\boldsymbol{v} = \sum_{n=1}^{N} \kappa_n(t)\widetilde{\boldsymbol{v}}_n. \tag{25}$$

Note that the expansion coefficients κ_n are functions of t since we are solving the full initial value problem of Equation 19 and not the restricted problem of Equation 23. We can restate Equation 19 in the simple form

$$\frac{\mathrm{d}\boldsymbol{\kappa}}{\mathrm{d}t} = -i\Lambda\boldsymbol{\kappa}, \quad \Lambda \in \mathbb{C}^{N \times N}, \quad \boldsymbol{\kappa} \in \mathbb{C}^N, \tag{26}$$

with

$$\boldsymbol{\kappa} = [\kappa_1 \ldots, \kappa_N]^{\mathrm{T}}, \qquad \Lambda = \mathrm{diag}[\omega_1 \ldots, \omega_N]. \tag{27}$$

The operator Λ represents the linear evolution operator, $\mathcal{M}^{-1}\mathcal{L}$, projected onto the space $\mathbb{S}^N$.

3.2. Energy Norm

In order to complete the transformation of the vector functions $\boldsymbol{v}$ to coefficients $\boldsymbol{\kappa}$, we must consider the scalar product and its associated norm. To measure the disturbance energy, we

consider the combination of the (nondimensional) disturbance kinetic and magnetic energies

$$E_V = \frac{1}{2} \int_V \left(|\boldsymbol{u}|^2 + |\boldsymbol{b}|^2 \right) \mathrm{d}V. \tag{28}$$

From Equation 9 we have

$$\mathcal{D}u + iku_z = 0, \qquad \mathcal{D}b + ikb_z = 0. \tag{29}$$

Therefore, by virtue of Parseval's equivalence (*e.g.* Tichmarsh, 1948), we can write

$$E_V = \int_k \frac{1}{2k^2} \int_{-d}^{d} \left(|\mathcal{D}u|^2 + k^2|u|^2 + |\mathcal{D}b|^2 + k^2|b|^2 \right) \mathrm{d}x \, \mathrm{d}k. \tag{30}$$

Following previous works (*e.g.* Reddy and Henningson, 1993), we take the energy density E as

$$E = \frac{1}{2k^2} \int_{-d}^{d} \left(|\mathcal{D}u|^2 + k^2|u|^2 + |\mathcal{D}b|^2 + k^2|b|^2 \right) \mathrm{d}x. \tag{31}$$

Since Equation 31 provides a sensible measure of the energy for a given k, we define the energy norm as

$$\|\boldsymbol{v}\|_{\mathrm{E}}^2 = \frac{1}{2k^2} \int_{-d}^{d} \left(|\mathcal{D}u|^2 + k^2|u|^2 + |\mathcal{D}b|^2 + k^2|b|^2 \right) \mathrm{d}x. \tag{32}$$

For any $\boldsymbol{v}_1, \boldsymbol{v}_2 \in \mathbb{S}^N$, the inner product associated with the above energy norm can be written as

$$(\boldsymbol{v}_1, \boldsymbol{v}_2)_{\mathrm{E}} = \frac{1}{2k^2} \int_{-d}^{d} \boldsymbol{v}_2^H \mathcal{Q} \boldsymbol{v}_1 \, \mathrm{d}x, \tag{33}$$

where

$$\mathcal{Q} = \begin{pmatrix} k^2 - \mathcal{D}^2 & 0 \\ 0 & k^2 - \mathcal{D}^2 \end{pmatrix}, \tag{34}$$

and the superscript H represents the complex-conjugate transpose. The integrands in Equations 32 and 33 can be related *via* integration by parts. Equation 33 can be written as

$$(\boldsymbol{v}_1, \boldsymbol{v}_2)_{\mathrm{E}} = \frac{1}{2k^2} \int_{-d}^{d} \boldsymbol{v}_2^H \mathcal{Q} \boldsymbol{v}_1 \, \mathrm{d}x = \boldsymbol{\kappa}^H Q \boldsymbol{\kappa}, \tag{35}$$

where the matrix Q has components

$$Q_{ij} = (\widetilde{\boldsymbol{v}}_i, \widetilde{\boldsymbol{v}}_j)_{\mathrm{E}} = \frac{1}{2k^2} \int_{-d}^{d} \widetilde{\boldsymbol{v}}_j^H \mathcal{Q} \widetilde{\boldsymbol{v}}_i \, \mathrm{d}x. \tag{36}$$

The matrix Q is both Hermitian and positive definite. We can, therefore, factor Q according to $Q = F^H F$ (*e.g.* Trefethen and Bau, 1997), leading to

$$(\boldsymbol{v}_1, \boldsymbol{v}_2)_{\mathrm{E}} = \boldsymbol{\kappa}_2^H Q \boldsymbol{\kappa}_1 \tag{37}$$

$$= \boldsymbol{\kappa}_2^H F^H F \boldsymbol{\kappa}_1 \tag{38}$$

$$= (F\boldsymbol{\kappa}_1, F\boldsymbol{\kappa}_2)_2. \tag{39}$$

The associated vector norm satisfies

$$\|\boldsymbol{v}\|_{\mathrm{E}} = \|F\boldsymbol{\kappa}\|_2, \quad \boldsymbol{v} \in \mathbb{S}^N. \tag{40}$$

This relationship between the energy norm and the L^2 norm is useful for the practical calculation of the optimal energy growth that we discuss shortly.

3.3. Optimal Growth

The formal solution of the initial value problem 19 can be written as

$$\boldsymbol{v} = \exp(\mathcal{M}^{-1}\mathcal{L}t)\boldsymbol{v}_0, \quad \boldsymbol{v}_0 = \boldsymbol{v}(0). \tag{41}$$

Using Equation 25, we can transform the above result into

$$\boldsymbol{\kappa} = \exp(-i\,\Lambda t)\boldsymbol{\kappa}_0, \quad \boldsymbol{\kappa}_0 = \boldsymbol{\kappa}(0). \tag{42}$$

The optimal transient growth of the disturbance energy is given by the norm of the matrix exponential

$$G(t) \equiv G(t, S, k) = \max_{\boldsymbol{v}_0 \neq \boldsymbol{0}} \frac{\|\boldsymbol{v}(t)\|_{\mathrm{E}}^2}{\|\boldsymbol{v}_0\|_{\mathrm{E}}^2} \tag{43}$$

$$= \max_{\boldsymbol{\kappa}_0 \neq \boldsymbol{0}} \frac{\|F\boldsymbol{\kappa}(t)\|_2^2}{\|F\boldsymbol{\kappa}_0\|_2^2} \tag{44}$$

$$= \max_{\boldsymbol{\kappa}_0 \neq \boldsymbol{0}} \frac{\|F\exp(-i\,\Lambda t)\boldsymbol{\kappa}_0\|_2^2}{\|F\boldsymbol{\kappa}_0\|_2^2} \tag{45}$$

$$= \max_{\boldsymbol{\kappa}_0 \neq \boldsymbol{0}} \frac{\|F\exp(-i\,\Lambda t)F^{-1}F\boldsymbol{\kappa}_0\|_2^2}{\|F\boldsymbol{\kappa}_0\|_2^2} \tag{46}$$

$$= \|F\exp(-i\,\Lambda t)F^{-1}\|_2^2. \tag{47}$$

Equation 47 follows from Equation 46 *via* the definition of an induced norm.

The curve traced out by $G(t)$ *vs. t* represents the maximum possible energy amplification, which for each instant of time is optimized over all possible initial conditions with unit energy norm (Schmid and Henningson, 1994). The initial disturbance that optimizes the amplification factor can be different for different times. Therefore, $G(t)$ should be thought of as the envelope of the energy growth of individual initial conditions with unit energy norm. Henceforth, we refer to $G(t)$ as the optimal energy envelope.

4. Numerical Procedure

In this section we briefly outline the main numerical procedures for the required calculations. Until now, we have presented the theory in terms of the underlying operators. Since a practical solution requires a (finite) discretization of the problem, we henceforth refer to matrices rather than operators and eigenvectors rather than eigenmodes. When referring back to an equation containing operators, it will be implicit that we are now considering the discretized version of that equation and, hence, are strictly dealing with finite matrices rather than operators.

4.1. Discretization for the Eigenvalue Problem

We follow previous works on non-normal stability by expanding the variables in terms of Chebyshev polynomials. These functions are defined in the interval $[-1, 1]$. It is trivial to convert from the problem domain $[-d, d]$ into the Chebyshev domain *via* $y = x/d$, with $y \in [-1, 1]$. A function can be approximated on the Chebyshev interval as

$$f(y) = \sum_{n=0}^{N} a_n T_n(y), \tag{48}$$

where

$$T_n(y) = \cos\left[n \cos^{-1}(y)\right] \tag{49}$$

and the a_n are constants. The unknown variables u and b in Equation 19 are expanded in the form of Equation 48. Derivatives are also expressed in terms of Chebyshev polynomials and make use of standard recurrence relations (*e.g.* Abramowitz and Stegun, 1964). In order to use these recurrence relations, the expanded equations are then required to be satisfied at the Gauss–Lobatto collocation points,

$$y_j = \cos\left(\frac{\pi j}{N}\right). \tag{50}$$

If we consider the eigenvalue problem of Equation 23, the expansion in terms of Chebyshev polynomials produces a matrix–vector system where the matrices (for the generalized eigenvalue problem) contain spectral differentiation matrices and the vector contains the expansion coefficients a_n.

Boundary conditions are included in rows of one of the matrices of the discretized generalized eigenvalue problem. The corresponding rows in the other matrix are chosen to be a complex multiple of these rows. By choosing a large complex multiple, spurious modes associated with the boundary conditions can be mapped to a part on the complex plane far from the region of interest (far below the eigenvalues near $\Im(\omega) = 0$). To illustrate this approach, consider the discrete form of Equation 23

$$-i\omega M\boldsymbol{x} = L\boldsymbol{x}, \tag{51}$$

where M and L are finite matrices and $\boldsymbol{x}$ represents an eigenvector. We can write

$$M = \begin{pmatrix} T_0(1) & T_1(1) & \dots \\ T_0''(y_1) - k^2 T_0(y_1) & T_1''(y_1) - k^2 T_1(y_1) & \dots \\ \vdots & \vdots & \vdots \\ T_0''(y_{N-1}) - k^2 T_0(y_{N-1}) & T_1''(y_{N-1}) - k^2 T_1(y_{N-1}) & \dots \\ T_0(-1) & T_1(-1) & \dots \\ \vdots & \vdots & \ddots \end{pmatrix}, \tag{52}$$

where we indicate the layout of the top-left section of the matrix (see the definition of $\mathcal{M}$ in Equation 20). Boundary conditions have been included in the 1st and Nth rows. The same rows in L are chosen as a complex multiple of the corresponding rows in M (Reddy, Schmid,

and Henningson, 1993). In this article, we multiply the rows by $-8000i$. For brevity, we do not display the full matrix of the discretized problem.

Once the system is fully discretized, the generalized eigenvalue problem can be solved by standard methods. In this article, we perform the calculations in MATLAB.

4.2. Optimal Quantities

4.2.1. Energy Growth

To calculate the optimal energy growth, we make use of singular value decomposition (SVD). Writing $A = F \exp(-i \Lambda t) F^{-1}$, we can decompose this matrix as

$$AV = \Sigma U, \tag{53}$$

where U and V are unitary matrices and Σ is a matrix containing the singular values, ordered by size. It can be shown that $\|A\|_2 = \sigma_1$, where σ_1 is the highest singular value of A (*e.g.* Trefethen and Bau, 1997). *Via* Equation 47, we use this property to determine the optimal energy growth. Again, we use MATLAB to calculate the SVD.

4.2.2. Optimal Disturbances

In order to determine the initial disturbance that will create the maximum possible amplification at a given time t_0, we can make further use of the SVD. Let $A = F \exp(-i \Lambda t_0) F^{-1}$. If σ_1 is the highest singular value of A, then, as described above,

$$\sigma_1 = \left\| F \exp(-i \Lambda t_0) F^{-1} \right\|_2 = \left\| \exp(-i \Lambda t_0) \right\|_E. \tag{54}$$

If we perform a decomposition, as before, and now focus only on the column vectors of U and V corresponding to σ_1, we obtain

$$A \boldsymbol{v}_1 = \sigma_1 \boldsymbol{u}_1. \tag{55}$$

The effect of A on an input vector $\boldsymbol{v}_1$ results in an output vector $\boldsymbol{u}_1$ stretched by a factor of σ_1. That is, $\boldsymbol{v}_1$ represents an initial condition that will be amplified by a factor σ_1 due to the mapping $F \exp(-i \Lambda t_0) F^{-1}$, where t_0 is the time when the amplification is reached (*e.g.* Schmid and Henningson, 1994). On the subspace $\mathbb{S}^N$, the optimal initial disturbance can be expressed as

$$\boldsymbol{\kappa}_1 = F^{-1} \boldsymbol{v}_1. \tag{56}$$

5. Spectra and Perturbed Matrices

In this section we present some of the results from solving the generalized eigenvalue problem of Equation 23. To be more precise, we solve the discretized version of Equation 23 subject to the numerical scheme outlined in the previous section. Throughout the rest of the article, unless specified otherwise, we set $d = 10$. Let us consider $S = 1000$ and examine the spectra for the cases $k = 0.5$ and $k = 1.2$. Figure 1 displays these two spectra.

For the tearing problem set up in this article, it can be shown analytically that the equilibrium can only become tearing-unstable for $0 < k < 1$. The spectrum in Figure 1a is for

Figure 1 Spectra for the discrete generalized eigenvalue problem, Equation 23, for $S = 1000$ and (**a**) $k = 0.5$ and (**b**) $k = 1.2$. In (**a**), the unique eigenvalue corresponding to the tearing mode is highlighted.
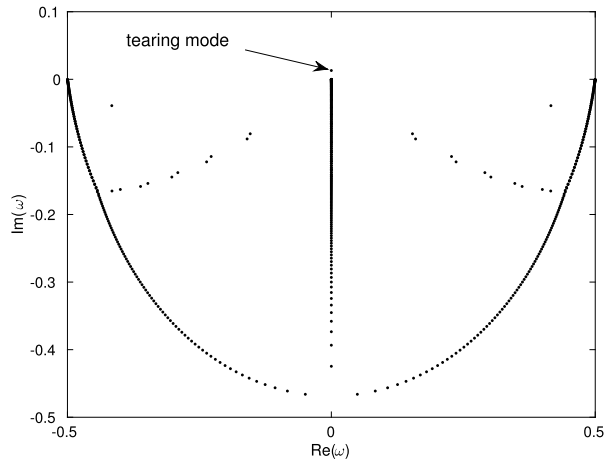

(a)
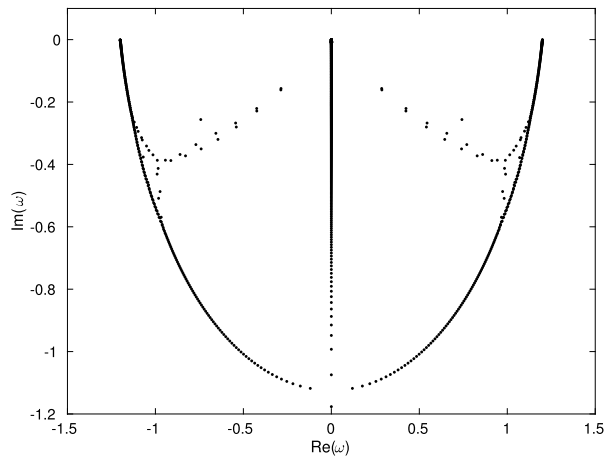
(b)

$k = 0.5$ and the system is, therefore, linearly unstable to the tearing instability. As can be seen from this spectrum, there is only one unstable eigenvalue, labelled as corresponding to the tearing mode. This eigenvalue is ≈ 0.0131, which is equivalent to the value obtained from a finite-difference solution of the same problem (Hood, private communication). The layout of the spectrum is qualitatively similar to other tearing-unstable spectra that have been calculated for similar boundary conditions and background equilibria (*e.g.* Goedbloed, Keppens, and Poedts, 2010). There is a distinct branching structure that is found in the spectra of many non-normal matrices (Reddy, Schmid, and Henningson, 1993).

In the spectrum for $k = 1.2$, in Figure 1b, there are no eigenvalues with $\Im(\omega) > 0$. There is still, however, a branching structure similar to the previous spectrum. The branch points of the spectra indicate the non-normal behavior of this resistive MHD problem. This means that eigenvectors with eigenvalues satisfying $\Im(\omega) < 0$ can contribute transient growth to the amplification of energy. In order to reveal this non-normal behavior, consider the following

Figure 2 Same spectra as in
Figure 1, but now with
eigenvalues of the perturbed
matrices included and shown in
red.
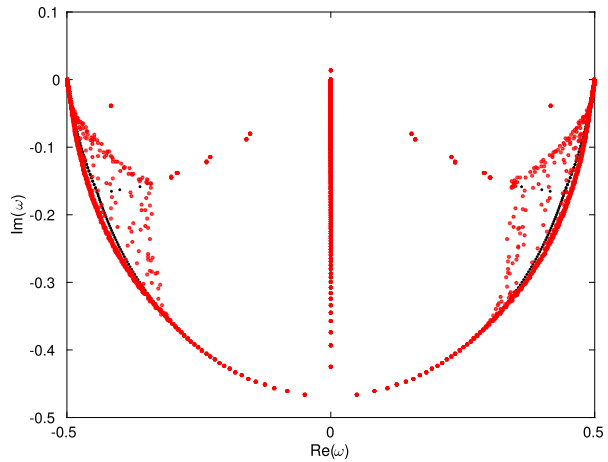
(a)
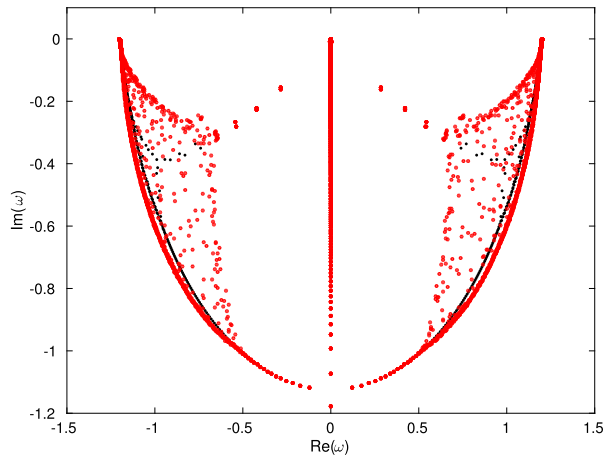
(b)

description. Let A be a matrix from which the eigenvalues of the problem are found, and
let E be a matrix such that $\|E\|_2 \leq 1$. Consider, also, a small parameter $\epsilon \ll 1$. A complex
number, z, is in the pseudospectrum of A, $\sigma_\epsilon(A)$, if z is in the spectrum of $A + \epsilon E$ (a similar
statement can be made for finite operators). For a normal matrix, points $z \in \sigma_\epsilon$ can differ
from corresponding points in the spectrum of A by $O(\epsilon)$, *i.e.* by the size of the perturbation
(*e.g.* Trefethen and Embree, 2005).

For a non-normal matrix, however, the difference can be much larger. Instead of the
eigenvalues of $A + \epsilon E$ differing from those of A by, at most, $O(\epsilon)$, they can differ by $O(1)$.
This behavior is particularly present at the branch points of spectra.

If A represents the unperturbed matrix of the spectra displayed in Figure 1, Figure 2
displays the spectra of $A + \epsilon E$ (for $k = 0.5, 1.2$) where $\epsilon = O(10^{-6})$ and the entries of
E are random and taken from a normal distribution. The eigenvalues of $A + \epsilon E$, for six
different random matrices E, are shown in red.

The pseudospectrum of A would be the subset of the complex plane given by

$$\sigma_\epsilon = \bigcup_{\|E\|_2 \leq 1} \sigma(A + \epsilon E). \tag{57}$$

As demonstrated in Figure 2, however, only a few matrices E are required to reveal the non-normal character of the matrix A.

There are several equivalent definitions of pseudospectra (Trefethen and Embree, 2005). The definition we have presented here gives the simplest and most practical demonstration of non-normal behavior. For our current purposes, this version of the pseudospectrum will suffice.

Looking at the eigenvalues of the perturbed matrix, there are two main features that emerge. The first is that for large parts of the spectra, the eigenvalues of $A + \epsilon E$ differ from the eigenvalues A by $O(\epsilon)$, indicating normal behavior. The second feature is that near the branch points of the spectra, the difference is now much larger. For both spectra displayed, a perturbation of $O(10^{-6})$ produces a difference of $O(10^{-1})$ between the eigenvalues of the matrices A and $A + \epsilon E$ at the branch locations. This jump of five orders of magnitude is a clear signal of non-normality and, hence, the possibility of significant transient growth. Estimating the pseudospectrum of Equation 57 with just a few random matrices E is the recommended approach for determining if the system in question is non-normal since it is easily determined from the spectrum that we use for determining the optimal transient growth. Plotting the pseudospectrum estimate, as done in Figure 2, also reveals what eigenvectors will produce non-normal effects and then should, therefore, be included in the subspace $\mathbb{S}^N$.

6. Optimal Energy Growth

6.1. Spectrally Stable k

As stated previously, the onset of the tearing instability, for the present setup, occurs only for $0 < k < 1$ in normal-mode analysis. However, as demonstrated in the previous section, the system is non-normal and allows for the possibility of transient growth, even for $k > 1$. To get an overview of the optimal energy growth for spectrally stable k, we calculate $\max_{t \geq 0} G(t)$ for different k. For the calculation of $G(t)$, we only consider contributions from eigenvalues with $-1.4 < \Im(\omega) < 0$. This means that for different values of k, different numbers of eigenvalues (and therefore eigenvectors) are used in the calculations. However, this range captures most of the effects of the non-normality, as suggested by the pseudospectra, and does not disguise the main results. The values of $\max_{t \geq 0} G(t)$ for a range of $k > 1$ and for the cases $S = 100$ and $S = 1000$ are displayed in Table 1.

Table 1 Maxima of $G(t)$ in time for $k > 1$ and magnetic Lundquist numbers $S = 100, 1000$.

k	$\max G(t, S = 100)$	$\max G(t, S = 1000)$
1.1	1.6	8.48
1.2	1.51	10.86
1.3	1.41	11.79
1.4	1.35	11.42
1.5	1.29	11.57

Figure 3 Example of an optimal energy envelope $G(t)$ for $S = 1000$ and $k = 1.1$.
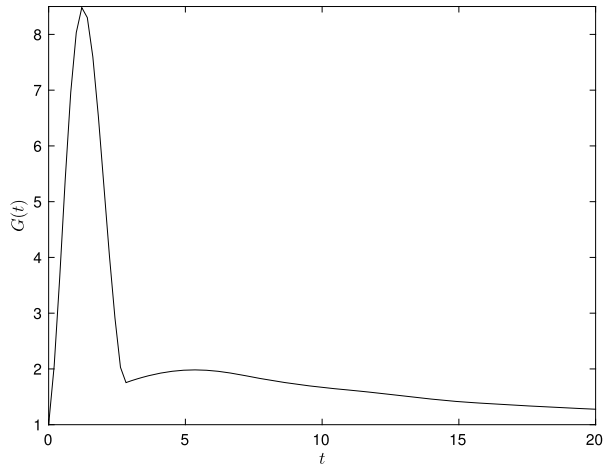
Table 2 S *vs.* $\kappa(F)$ for $k = 1.1$.

S	10	50	100	500	1000	5000
$\kappa(F)$	20	690	1.6×10^4	2×10^8	3×10^8	3.8×10^8

For $S = 100$, the optimal energy growth is small and does not even double in size for the values of k displayed. This result is important as the magnetic Lundquist number for many simulations can be of O(100). Therefore, any transient growth would not be noticed. Moving up to $S = 1000$, the optimal energy growth can increase by an order of magnitude. In the solar corona, where $S \approx$ O(10^8) and higher, it is therefore possible that transient growth for spectrally stable k could become large enough to excite the nonlinear phase of the tearing instability. An example of a $G(t)$ envelope for $k = 1.1$, $S = 1000$ is shown in Figure 3.

In light of the results of Table 1, we may ask how the transient energy growth can increase with increasing S. One way to answer this question is to consider a simple upper bound for the energy growth. For an initial value problem, suppose that ω_{I} is the imaginary part of the least damped eigenvalue of Λ. It then follows that

$$\exp(\omega_{\mathrm{I}}t) \leq \left\| \exp(-i\Lambda t) \right\|_{\mathrm{E}} \tag{58}$$

$$\leq \|F\|_2 \left\| F^{-1} \right\|_2 \exp(\omega_{\mathrm{I}}t) \tag{59}$$

$$\leq \kappa(F) \exp(\omega_{\mathrm{I}}t), \tag{60}$$

where $\kappa(F) = \|F\|_2 \|F^{-1}\|_2$ is the standard notation for the condition number of the matrix F (not to be confused with κ from Equation 25). If $\kappa(F) = 1$ in Equation 60, we have equality and the energy bound is determined by the least damped eigenvalue alone. If, however, $\kappa(F) \gg 1$, then there is the potential for substantially larger energy growth at early times, even though it may be that $\omega_{\mathrm{I}} < 0$. For the tearing-stable case studied above, $\omega_{\mathrm{I}} \approx 0$ and so the energy bound is given by $\kappa(F)$. Table 2 shows how the condition number varies for some values of S when $k = 1.1$.

Clearly, using $\kappa(F)$ as an upper bound for the energy is too loose for practical considerations. However, the purpose of displaying these results is to convey the following: as S increases and, hence, the diffusion term in the induction equation is multiplied by a smaller

Figure 4 Optimal energy growth curves $G(t)$ for $S = 1000$ and $k = 0.2$. Key: $\Im(\omega) > -0.6$ (*solid*), $\Im(\omega) > 0$ (*dash*).
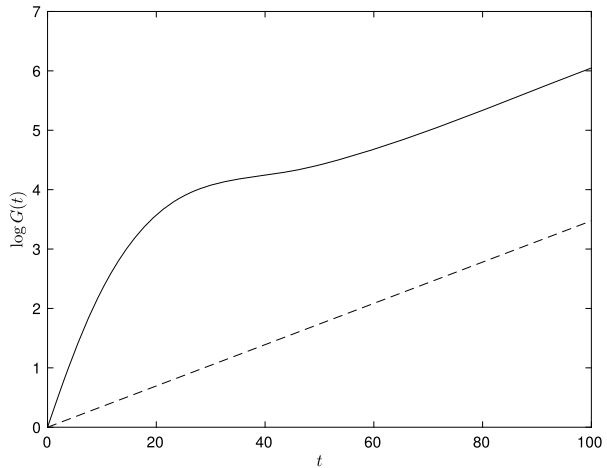
coefficient S^{-1}, it may reasonably be expected that the energy bound tends to an ideal MHD limit, where the onset of instability is governed entirely by eigenvalues. However, the opposite is true, allowing for (non-normal) transient effects to play a significant role. As S increases, the eigenvectors (related to F *via* the inner product in Equation 39) become more ill-conditioned, as discussed in Bobra *et al.* (1994).

Stricter bounds (both upper and lower) for the energy growth can be determined using pseudospectral theory (Trefethen and Embree, 2005). However, such considerations go beyond the scope of the present article and will be considered in future work.

6.2. Spectrally Unstable k

For $0 < k < 1$, a normal-mode analysis would produce the eigenvalue with the highest positive value of $\Im(\omega)$, which would represent the growth rate of the linearly unstable system. For the tearing instability, the growth rate behaves as $S^{-\alpha}$ for $0 < \alpha < 1$, which, for coronal values, is very slow. For a discussion of the various values of α, determined by eigenvalue analysis in different regimes, we refer to Tenerani *et al.* (2016).

Since normal-mode analysis ignores any energy growth that decays as $t \to 0$, the possibility of faster energy growth due to transient effects is often neglected. To demonstrate the possible effect of transients on the growth rate, Figure 4 displays the optimal energy growth envelopes for two cases: the optimal energy growth due to the tearing mode alone, and the optimal energy growth due to the combination of the tearing mode and spectrally stable eigenvectors. This example is calculated for $S = 1000$ and $k = 0.2$, and when transient effects are included, we consider eigenvectors with corresponding eigenvalues with imaginary parts bounded below by $\Im(\omega) = -0.6$.

The dashed curve represents the optimal energy growth using only the tearing mode. This envelope could be produced if we performed a normal-mode analysis. Comparing this curve to the case where other eigenvectors are included in the calculation reveals very interesting behavior. By $t \approx 20$, $G(t)$ from the solid curve increases to ≈ 30 (note that the Figure displays $\log G(t)$), compared to that of the dashed curve, which only increases to ≈ 1. Including the effects of transient growth has resulted in an optimal energy growth that proceeds much more rapidly, at short times, compared to the contribution from the linearly unstable mode alone. By $t \approx 40$, the solid curve begins to plateau and the growth rate is now

slower than that of the dashed curve. This is due to the initial transients decaying and having weaker effect on the energy growth. From $t \approx 60$ and beyond, both curves become parallel. This behavior is to be expected as the contribution from the unstable mode dominates as $t \to \infty$. It is clear from Figure 4 that including the effects of the transients can increase the optimal energy growth substantially.

As mentioned before, the curves of $G(t)$ are envelopes of the optimal energy growth and so, in practice, they may not be reached if the initial perturbation is not optimal. However, Figure 4 reveals that even if the optimal energy growth is not attained, the gap between the envelopes for growth with and without transient effects can be large. Hence, even a non-optimal perturbation can produce fast energy growth that could amplify the energy to an order of magnitude (or more) greater than that predicted by normal-mode analysis, within a given time.

6.3. Optimal Disturbances

The optimal energy envelopes described in the last section represent, at every point in time, the energy amplification optimized over all initial conditions with unit energy norm. As described in Section 4.2.2, we can determine the optimal perturbation from the same analysis used to calculate $G(t)$. That is, for a given time, we can determine the initial perturbation that produces the optimal energy amplification at that time. To illustrate this, Figure 5 shows the optimal initial values for the x-component of the velocity at times $t = 30, 40$ for the case $S = 1000, k = 0.2$.

The other components of $\boldsymbol{u}$ and $\boldsymbol{b}$ at $t = 0$ can also be found. For brevity, we omit displaying them here. The purpose of calculating the optimal initial conditions is described in the following section.

7. Discussion

7.1. Summary

In this article, we have demonstrated that the linear onset of the tearing instability can exhibit large transient energy growth due to the non-normality of the associated resistive MHD operator. This energy amplification is found by solving the full initial value problem rather than just the eigenvalue problem of normal-mode analysis. The latter theory is only concerned with the asymptotic growth of the linear system and ignores transient effects. From our illustrative examples we have shown that transient energy growth can be amplified much faster than that determined purely from normal-mode analysis. This behavior has been demonstrated for both tearing-stable and tearing-unstable values of the wavenumber.

To determine the optimal energy growth, we have made use of the eigenvalues and eigenvectors of the system. By plotting pseudospectra, we revealed that a subset of eigenvectors contributes to transient energy growth. The eigenvectors of this subset have eigenvalues ω with $\Im(\omega) < 0$, which are ignored by normal-mode analysis.

The optimal energy envelopes that we calculated increase in amplitude with the magnetic Lundquist number S. These curves represent the possible energy amplification that can be achieved if the initial condition is optimal. However, even if the initial condition is not optimal, there is still the possibility for energy growth that is much faster than the growth rate determined from normal-mode analysis. This means that transient energy growth could, potentially, trigger the nonlinear phase of the tearing instability much sooner than previously expected. If this is the case, the implications for the tearing instability in solar physics would be substantial.

Figure 5 Optimal initial u_x for (**a**) $t = 30$, (**b**) $t = 40$.
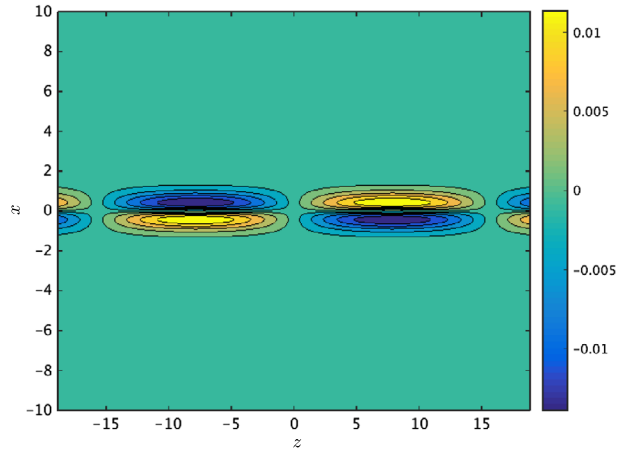
(a)
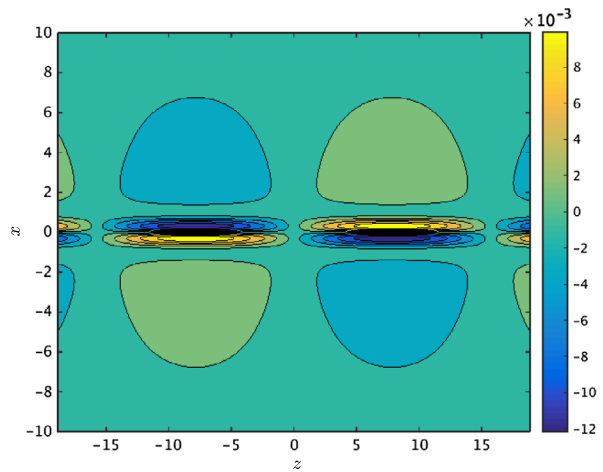
(b)

7.2. Solar Applications

7.2.1. Coronal Phenomena

In the solar corona, two important phenomena that are often linked to current sheets and their dissipation are coronal heating and solar eruptions. For the first of these, the "nanoflare" theory suggests that the corona is heated by many "small" heating events (or flares) spread throughout the coronal magnetic field (Parker, 1988). The tearing of current sheets, which develop from the complex deformation of magnetic fields, is one possible way that the magnetic field can release its energy as heat. Recent models of the nonlinear development of the MHD kink instability have revealed the development of many small-scale current features that could act as nanoflares (*e.g.* Hood *et al.*, 2016). Our results support the idea of coronal heating *via* tearing instabilities as perturbations could excite large transient growth, which, in turn, could potentially readily generate nanoflares.

For the second phenomenon, current sheets are believed to play an important role at the onset, and subsequent nonlinear development, of solar eruptions. Such current sheets would be manifest in the flares associated with the initiation of CMEs, jets, and surges. Simulations of CME-type eruptions often reveal a combination of reconnection above and below the CME, referred to as the breakout theory of CMEs. In particular, simulations, both 2D and 3D, demonstrate that tearing reconnection above and below the CME heralds the onset of an eruption (*e.g.* MacNeice *et al.*, 2004; MacTaggart and Haynes, 2014). The onset of jets and surges has also been linked to the tearing of current sheets (*e.g.* MacTaggart *et al.*, 2015). The onset of jets and eruptions is an important topic, not only for theoretical interest, but for space weather applications. Therefore, understanding all aspects (normal and non-normal) of the onset of the tearing instability is vital.

7.2.2. Quasi-Singular Current Sheets and the Plasmoid Instability

Recent work by Pucci and Velli (2014) has highlighted that the aspect ratio of current sheets has a threshold value after which equilibrium cannot be reached and the current sheet must reconnect. Various simulations have revealed that a fast tearing instability can develop for large S and have growth rates proportional to $S^{1/4}$ (Lourerio, Schekochihin, and Cowley, 2007; Lapenta, 2008). Hence, in the limit as $S \to \infty$, there would be, in the words of Pucci and Velli (2014), an "infinitely unstable mode", which is impossible in ideal MHD. By a simple and clever scaling argument, they showed that once the current sheet aspect ratio is $O(S^{1/3})$, a laminar current sheet cannot be supported and fast tearing must proceed.

Although we agree with the main conclusion of Pucci and Velli (2014), we would suggest an alternative path to reaching their result. Their analysis is based entirely on eigenvalues and eigenvectors and so ignores the contribution of any transient growth. As the possible energy amplification of transient growth increases with S, a much faster onset of the tearing instability could be found that is due to transient growth. Such transient growth depends on the initial perturbation. Hence, the result of Pucci and Velli (2014) can be thought of as a lower bound, when there are no effects of transient growth. As soon as there are perturbations that can induce transient growth, energy amplification will grow faster, thus exciting the tearing instability faster, as shown in the example in Figure 4.

Further recent work by Comisso *et al.* (2016) attempts to describe a general theory of the plasmoid instability, formulated by means of a principle of least time. In their analysis, they find that the scaling relationships for the final aspect ratio, the transition time to rapid onset, the growth rate, and the number of plasmoids depend on the size of the initial disturbance amplitude, the rate of current sheet evolution, and the Lundquist number. We agree that the initial conditions are important for the onset of the instability, however, we would suggest that the theory of Comisso *et al.* (2016) could be extended to include transient effects like those described in this article. Using scalings for the tearing mode alone will not give a complete description of the transient phase of the instability.

7.3. Future Work

This work can proceed in two main directions. The first is to include extra physics (*e.g.* two fluid effects) to study how this would effect transient growth. The second, and perhaps most important, is to use optimal initial perturbations as initial conditions in nonlinear resistive MHD simulations. This task will determine if transient growth can lead to a fast nonlinear phase of the tearing instability or if nonlinear terms saturate the transient growth. It will

be particularly interesting to determine if the nonlinear tearing instability can be excited by perturbations with $k > 1$, *i.e.* spectrally stable perturbations.

Although we have suggested that our results can extend those of previous studies (such as Pucci and Velli, 2014 and Comisso *et al.*, 2016), there remains much further work to understand how the damped part of the eigenvalue spectrum perturbs the current sheet and drives reconnection, particularly at very high values of S.

Disclosure of Potential Conflicts of Interest   The authors declare that they have no conflicts of interest.

Appendix

Throughout this article, we have performed calculations with boundary conditions $u = b = 0$ at $x = \pm d$. This has been done so that our results can be easily compared to other works and to nonlinear simulations, which typically use such boundary conditions. Since the tearing instability develops in a boundary layer near $x = 0$, the precise nature of the boundary conditions should not play a strong role in the onset of the instability. To illustrate this, we solve the discrete form of Equation 23, with $S = 1000$ and $k = 0.5$, in the half-plane and compare the resulting spectrum to that in Figure 1a.

Anticipating a symmetric solution in b and an antisymmetric solution in u about $x = 0$, we set the boundary conditions at $x = 0$ to be

$$u = \frac{db}{dx} = 0. \tag{61}$$

As $x \to \infty$, we set

$$u = b = 0. \tag{62}$$

In order to represent this boundary numerically, we consider a large domain denoted by $0 \leq x \leq x_{\max}$. In order to expand the variables using Chebyshev polynomials, we need to map our coordinates to the domain $-1 \leq y \leq 1$. This is achieved through

$$x = a \frac{1+y}{b-y}, \tag{63}$$

where

$$a = \frac{x_{\max} x_i}{x_{\max} - 2x_i} \quad \text{and} \quad b = 1 + \frac{2a}{x_{\max}}. \tag{64}$$

This mapping clusters the grid points near the boundary layer at $x = 0$ and places half of the grid points in the region $0 \leq x \leq x_i$ (Hanifi, Schmid, and Henningson, 1996). In this example, we take $x_{\max} = 100$ and $x_i = 15$. The resulting spectrum is displayed in Figure 6.

By inspection, the comparison with Figure 1a yields few differences. The eigenvalue corresponding to the tearing mode now has a value ≈ 0.0111, which is still similar to that calculated for the other boundary conditions. Two isolated eigenvalues near $\Im(\omega) = 0$ in Figure 1a are now pushed nearer the main branches in Figure 6. Apart from these minor differences, the spectra calculated from different boundary conditions are very similar. This result suggests that the exact form of boundary conditions, assuming they do not interfere dynamically with the boundary layer at $x = 0$, will not radically change the behavior of the onset of the tearing instability.

Figure 6 Spectrum of the discrete eigenvalue problem with half-plane boundary conditions for $S = 1000$, $k = 0.5$.
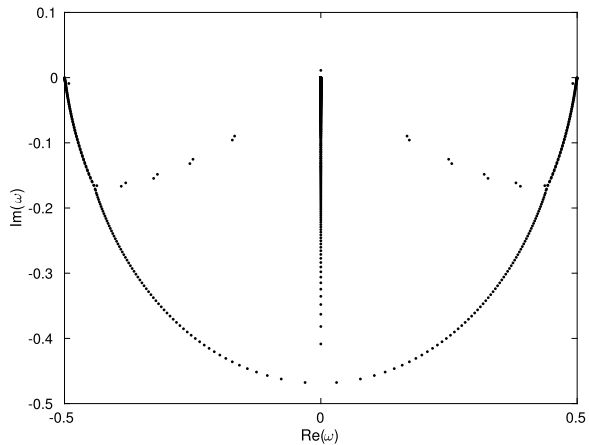
References

Abramowitz, M., Stegun, I.A. (eds.): 1964, *Handbook of Mathematical Functions*, Dover, New York.

Bobra, D., Riedel, K.S., Kerner, W., Huysmans, G.T.A., Ottaviani, M., Schmid, P.J.: 1994, *Phys. Plasmas* **1**, 3151.

Camporeale, E.: 2010, *Space Sci. Rev.* **172**, 397.

Camporeale, E., Burgess, D., Passot, T.: 2009, *Phys. Plasmas* **16**, 030703.

Chandrasekhar, S.: 1961, *Hydrodynamic and Hydromagnetic Stability*, Clarendon, Oxford.

Comisso, L., Lingam, M., Huang, Y.-M., Bhattacharjee, A.: 2016, *Phys. Plasmas* **23**, 100702.

Farrell, B.F., Ioannou, P.J.: 1999a, *Astrophys. J.* **522**, 1079.

Farrell, B.F., Ioannou, P.J.: 1999b, *Astrophys. J.* **522**, 1088.

Furth, H.P., Kileen, J., Rosenbluth, M.N.: 1963, *Phys. Fluids* **6**, 459.

Goedbloed, J.P., Keppens, R., Poedts, S.: 2010, *Advanced Magnetohydrodynamics*, Cambridge University Press, Cambridge.

Hanifi, A., Schmid, P.J., Henningson, D.S.: 1996, *Phys. Fluids* **8**, 826.

Hood, A.W., Hughes, D.W.: 2011, *Phys. Earth Planet. Inter.* **187**, 78.

Hood, A.W., Cargill, P.J., Browning, P.K., Tam, K.V.: 2016, *Astrophys. J. Lett.* **817**, 5.

Lapenta, G.: 2008, *Phys. Rev. Lett.* **100**, 235001.

Livermore, P.W., Jackson, A.: 2006, *Proc. Roy. Soc. A* **462**, 2457.

Lourerio, N.F., Schekochihin, A.A., Cowley, S.C.: 2007, *Phys. Plasmas* **14**, 100703.

MacNeice, P., Antiochos, S.K., Phillips, S., Spicer, D.S., DeVore, C.R., Olson, K.: 2004, *Astrophys. J.* **614**, 1028.

MacTaggart, D., Haynes, A.L.: 2014, *Mon. Not. Roy. Astron. Soc.* **438**, 1500.

MacTaggart, D., Guglielmino, S.L., Haynes, A.L., Simitev, R.D., Zuccarello, F.: 2015, *Astron. Astrophys.* **576**, A4.

Parker, E.N.: 1988, *Astrophys. J.* **330**, 474.

Priest, E.R.: 2014, *Magnetohydrodynamics of the Sun*, Cambridge University Press, Cambridge.

Pritchett, P.L., Lee, Y.C., Drake, J.F.: 1980, *Phys. Fluids* **23**, 1368.

Pucci, F., Velli, M.: 2014, *Astrophys. J. Lett.* **780**, L19.

Reddy, S.C., Henningson, D.S.: 1993, *J. Fluid Mech.* **252**, 209.

Reddy, S.C., Schmid, P.J., Henningson, D.S.: 1993, *SIAM J. Appl. Math.* **53**, 15.

Schindler, K.: 2006, *Physics of Space Plasma Activity*, Cambridge University Press, Cambridge.

Schmid, P.J., Henningson, D.S.: 1994, *J. Fluid Mech.* **277**, 197.

Tassi, E., Hastie, R.J., Porcelli, F.: 2007, *Phys. Plasmas* **14**, 9.

Tenerani, A., Rappazzo, A.F., Velli, M., Pucci, F.: 2015, *Astrophys. J.* **801**, 145.

Tenerani, A., Velli, M., Pucci, F., Landi, S., Rappazzo, A.F.: 2016, *J. Plasma Phys.* **82**, 535820501.

Terasawa, T.: 1983, *Geophys. Res. Lett.* **10**, 475.

Tichmarsh, E.C.: 1948, *Introduction to the Theory of Fourier Integrals*, Oxford University Press, London.

Trefethen, L.N., Bau, D.: 1997, *Numerical Linear Algebra*, SIAM, Philadelphia.

Trefethen, L.N., Embree, M.: 2005, *Spectra and Pseudospectra: The Behaviour of Nonnormal Matrices and Operators*, Princeton University Press, Princeton.